Photocatalysed (meth)acrylate polymerization by (antimony-doped) tin oxide nanoparticles and photoconduction of their crosslinked polymer nanoparticle composites

Please check the document version of this publication:

• A submitted manuscript is the version of the article upon submission and before peer-review. There can be important differences between the submitted version and the official published version of record. People interested in the research are advised to contact the author for the final version of the publication, or visit the DOI to the publisher's website.
• The final author version and the galley proof are versions of the publication after peer review.
• The final published version features the final layout of the paper including the volume, issue and page numbers.

Link to publication

Research Article

Photocatalysed (Meth)acrylate Polymerization by (Antimony-Doped) Tin Oxide Nanoparticles and Photoconduction of Their Crosslinked Polymer Nanoparticle Composites

J. C. M. Brokken-Zijp,[1] O. L. J. van Asselen,[2] W. E. Kleinjan,[1] R. van de Belt,[3] and G. de With[1]

[1] *Laboratory of Materials and Interface Chemistry, Eindhoven University of Technology, P.O. Box 513, 5600 MB Eindhoven, The Netherlands*
[2] *Laboratory of Polymer Technology, Eindhoven University of Technology, P.O. Box 513, 5600 MB Eindhoven, The Netherlands*
[3] *Kriya Materials B.V., P.O. Box 18, 6160 MD Geleen, The Netherlands*

Correspondence should be addressed to J. C. M. Brokken-Zijp, j.brokken@tue.nl

In the absence of another (photo)radical initiator Sb:SnO_2 nanoparticles ($0 \leq Sb \leq 13$ at %) photocatalyze during irradiation with UV light the radical polymerization of (meth)acrylate monomers. When cured hard and transparent (>98%) films with a low haze (<1%) are required, when these particles are grafted in advance with 3-methacryloxypropyltrimethoxysilane (MPS) and doped with Sb. Public knowledge about the photocatalytic properties of Sb:SnO_2 nanoparticles is hardly available. Therefore, the influence of particle concentration, surface groups, and Sb doping on the rate of C=C (meth)acrylate bond polymerization was determined with aid of real-time FT-IR spectroscopy. By using a wavelength of irradiation with a narrow bandgab (315 ± 5 nm) the influence of these factors on the quantum yield (Φ) and on polymer and particle network structure formation was determined. It is shown that Sb doping and MPS grafting of the particles lowers Φ. MPS grafting of the particles also influences the structure of the polymer network formed. Without Sb doping of these particles unwanted, photocatalytic side reactions occur. It is also shown that cured MPS-Sb:SnO_2/(meth)acrylate nanocomposites have photoconduction properties even when the particle concentration is as low as 1 vol.%. The results suggest that the Sb:SnO_2 (Sb > 0 at %) nanoparticles can be attractive fillers for other photocatalytic applications photorefractive materials, optoelectronic devices and sensors.

1. Introduction

Spherical nanoparticles of antimony-doped tin oxide (Sb: SnO_2) can be used to provide semiconducting properties to insulating polymers. This change in properties occurs when these particles form a percolating network structure through the polymer matrix [1–6] at a filler concentration higher than the percolation threshold. In a number of scouting experiments in which we studied the rate of curing of such Sb:SnO_2)/acrylate formulations, we noticed that *in the absence of* an organic photoinitiator UV curing also

occurred. Because Sb:SnO_2 nanoparticles absorb UV light these results suggest that Sb:SnO_2 nanoparticles can act as photoinitiator for acrylate polymerization.

Photocatalytic effects have been reported for a number of semiconductive nanoparticles. For instance, Fe[III] doped TiO_2 can act as a photocatalyst in acrylate polymerization [7] and CdS [8] or ZnO [9] in methacrylate polymerization. It was also shown that the photocatalytic properties of TiO_2 can shorten the lifetime of TiO_2 polymer composites [10]. Furthermore, by absorption of UV radiation SnO_2 particles can oxidize organic molecules [11, 12], which

indicates that SnO_2 particles may also act as photocatalysts for (meth)acrylate polymerization. However, as far as we know, no literature is available on the properties of SnO_2 and $Sb:SnO_2$ (nano)particles to initiate radical polymerization, or on the photocatalytic properties of $Sb:SnO_2$ particles in general. Moreover, this study will give also insight into the possibility of using these semiconductor nanoparticles in a broad range of other applications, such as vapour and water purification, destruction of (unwanted) biological materials, water splitting for energy conversion applications and photorefractive materials [13–15], and the use of SnO_2 and $SbSnO_2$ for short wavelength optoelectronic devices [16].

It has been shown before that in the presence of an standard organic photoinitiator $Sb:SnO_2$/acrylate formulations are polymerized when these formulations are irradiated with UV light [1–6]. Most of these authors assume that the presence of the organic photoinitiator is essential for the occurrence of these photocatalyzed reactions. This is, however, not true. Moreover, when we studied these formulations in more detail, very complex results were obtained. Therefore we decided to focus the initial part of our research on the capability of SnO_2 and $Sb:SnO_2$ (nano)particles to photocatalyze the polymerization of (meth)acrylate monomers in the absence of any other (organic) photoinitiator and irradiated these formulations with UV light of $315 \, nm \pm 5 \, nm$. The energy of these light quanta is sufficient to transfer electrons from the valence band directly into the conduction band [17, 18].

For convenience, we will refer below to both SnO_2 and $Sb:SnO_2$ nanoparticles as $Sb:SnO_2$ nanoparticles and will specify when needed the amount of Sb present (0, 2, 7, 13 at %). We will demonstrate that these nanoparticles in the absence of any other (organic) photoinitiator photocatalyze the (meth)acrylate C=C polymerization during irradiation with UV light. We will propose a mechanism for these photocatalytic radical polymerizations and assess the influence of particle concentration and Sb doping of the particles on the polymerization rate and the quantum yield for the initiating radical formation. We will show that the presence of 3-metacryloxypropyltrimethoxysilane (MPS) surface groups and Sb doping of the nanoparticles are essential to prevent the occurrence of photocatalyzed site reactions and for the formation of highly transparent (>98%) cured films with low haze (<1%).

We also studied the photoconduction properties of the cured MPS-$Sb:SnO_2$/(meth)acrylate nanocomposites and relate the photoconduction properties of cured MPS-$Sb: SnO_2$/(meth)acrylate nanocomposites with the photocatalytic properties of MPS-$Sb:SnO_2$/(meth)acrylate starting formulations. That semiconductive inorganic nanoparticles, such as CdSe and CdS, in a polymer matrix can transfer an electron after absorption of light quanta of sufficient energy has been shown before [19, 20] and this property of inorganic semiconductive nanoparticles is used for instance, for developing photorefractive materials for optical data storage and dynamic processing. To our knowledge the occurrence of photoconduction in $Sb:SnO_2$ (Sb $\geq$ 0)/polymer nanocomposites or $Sb:SnO_2$ films has not been reported before.

2. Experimental

2.1. Chemicals and Materials Used.
Polyethyleneglycol diacrylate monomer (PEGDA) was purchased from Aldrich, 3-metacryloxypropyltrimethoxysilane (MPS) from ABCR, and methanol (>99.8%) from Merck (Scheme 1). Aqueous dispersions of $Sb:SnO_2$ nanoparticles ($\approx$10 wt%) with different Sb doping levels from Sb/(Sb+Sn) = 0 to 13.0 at. % (after this described as % Sb) were obtained from Kriya Materials B.V. (Geleen, The Netherlands). The most important properties of the $Sb:SnO_2$ particles used are summarized in Table 1 [4].

In general, the surface of the $Sb:SnO_2$ nanoparticles was modified in advance by grafting them with the coupling agent 3-methacryloxypropyltrimethoxysilane (MPS) in dispersion (Scheme 2) [21]. During grafting also an alcohol/water solvent switch was applied. The MPS/$Sb:SnO_2$ ratio used was between 0.045 g/g and 0.19 g/g (Scheme 2). Sometimes also MPS oligomers were formed in the dispersion. The total amount of MPS present in the dried $Sb:SnO_2$ powder and the grafted amount of MPS was determined by analyzing the total amount of C ($\mu mol \, m^{-2}$) present before and after separating the MPS oligomer using ultracentrifuging [4, 21]. The C amount was determined using elemental analysis on the carbon content (wt.%) combined with BET measurements [4]. The elemental analysis on the carbon content was performed with Euro EA 3000 element analyzer (Euro Vector Instruments & Software, Milan, Italy). The C amount found after grafting was corrected for the small amounts of C present before grafting. NH_3 groups are also present on the surface of the $Sb:SnO_2$ particles before grafting [4]. Using the same combination of analyses as for determining the amount of MPS, it was shown that the amount of NH_3 is not changed by the MPS grafting reaction.

2.2. Preparation of the (MPS) Sb:SnO₂ (Sb ≥ 0)/PEGDA Dispersions and Starting Formulations.
The water dispersions of $Sb:SnO_2$ (Sb = 0) nanoparticles (pH = 7) and the alcohol dispersions of the MPS-grafted $Sb:SnO_2$ nanoparticles were mixed with PEGDA 575 using a spatula and then diluted with methanol. Initially, the mass ratio between solvent and components (PEGDA, MPS and $Sb:SnO_2$ particles) was kept at 90/10 in these $Sb:SnO_2$/PEGDA dispersions. From these mixtures the starting formulation was made by placing these dispersions on the diamond crystal of the Golden Gate ATR accessory of our IR apparatus and then evaporating the solvents under a gentle dry nitrogen flow.

The $Sb:SnO_2$ particle content in the resulting composite (after evaporation of the solvent and curing with UV radiation) was varied between 0–10 vol%, based on the total amount of PEGDA, $Sb:SnO_2$, and MPS added. After grafting the MPS/$Sb:SnO_2$ ratio is smaller, because during grafting the MPS molecules lose methoxy groups (Scheme 2). We take this effect into account in determining the particle concentration in the cured composite material.

2.3. Measurement of the Curing Rate.
The FT-IR measurements were performed using a Biorad Excalibur FT-IR

MPS; $M_w = 248$ g/mol   PEGDA 575; $n_{av} = 9.2$; $M_w = 575$ g/mol
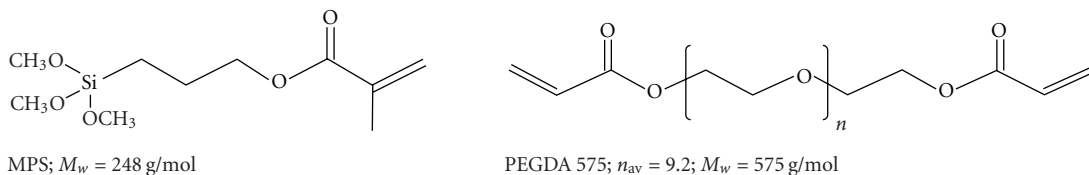
Scheme 1: 3-metacryloxypropyltrimethoxysilane (MPS) and Polyethyleneglycol diacrylate (PEGDA).

Table 1: Properties of the Sb:SnO$_2$ particles used [4].

Sb/(Sn + Sb) at %[a]	Sb(III)/[Sb(III)+Sb(V)] at %	d(nm)		N[b] wt.% E.A.	Powder Conductivity S/cm at R.T.
		BET[c]	XRD[d]		
0	0	8.2	7.3	0.134	$1.5 \cdot 10^{-5}$
2.0	0	7.9	6.9	0.204	$8.0 \cdot 10^{-5}$
7.0	0[e]	7.1	6.5	0.282	$4.5 \cdot 10^{-3}$
13.0	7.6	6.6	6.9[f]	0.402	$1.0 \cdot 10^{-2}$

[a] Apart from Sb 0% all the Sb:SnO$_2$ particles are blue powders.
[b] Present in the bulk and at the surface; at the surface as NH$_3$ groups.
[c] To calculate the diameter it was assumed that the particles were spherical, non-porous and had a density of 6.99 g/cm^3.
[d] The crystallite sizes were calculated from the broadening of the peaks.
[e] No Sb(III) were detected with XRD; IR data suggest that a very small amount of Sb(III)-OH groups are present on the surface.
[f] Measured with TEM: $d = 6.3 \pm 1.1$ nm.

spectrometer, equipped with an MCT detector. This instrument recorded the spectra in the kinetic mode over the spectral range from 650 to 4000 cm^{-1} with time intervals varying between 0.3–30 s, depending on the total time needed to reach full C=C bond conversion. An Oriel Spectral Luminator connected to a light guide was used to initiate the polymerization reaction. The used radiation wavelength was 315 ($\pm$5) nm. The incident light intensity I_0 just above the starting formulation was 0.5 (mW cm^{-2})(Oriel 70260 Radiant Power Meter).

The rate of polymerization of the PEGDA monomer and the MPS moieties in the starting formulation was measured as follows. Before irradiation a drop of the Sb: SnO$_2$/PEGDA dispersion was placed on the diamond crystal of the Golden Gate Attenuated Total Reflection (ATR) accessory, then the solvents present in this dispersion were evaporated under a gentle dry nitrogen flow, and the thickness of the starting formulation was adjusted so that the evanescent wave of the IR radiation penetrates through the whole sample. Then the electronic shutter of the UV lamp was opened ($t = 0$), and the polymerization rate of the C=C double bonds was followed by recording the decreases in the IR absorption(s) of the peaks at 1408, 1620, and 1637 cm^{-1} at different time intervals. During these measurements the dry nitrogen flow was kept on, and the shutter of the lamp was left open. The penetration depth of the radiation during the measurements was the same, and an internal standard for calculating the rates was therefore not required.

The initial rates of C=C bond disappearance were determined from the measured decrease in C=C bond absorptions at 1637, 1620, and 1408 cm^{-1} at the early stage of the reaction. Each decrease in C=C bond absorption was plotted in the form of a decrease in concentration from time $t = 0$ to time t (R_{ini}; (1)) or in the form of a relative decrease in absorption from time $t = 0$ to time t (R_{ini}^m; (2)). This latter approach was used when reaction rates were compared of Sb:SnO$_2$/PEGDA starting formulations which contained different starting amounts of C=C double bonds. The maximum rates (R_{max}, R_{max}^m) were determined as the maximum slope of the plots of, respectively, of the decrease in absorption (3) or the relative decrease in absorption versus time period $t_2 - t_1$ (4).

$$R_{ini} = \{c_{(C=C)t=0} - c_{(C=C)t}\} t^{-1} \ (\text{mol m}^{-3}\text{s}^{-1}) \qquad (1)$$

$$R_{ini}^m = \{c_{(C=C)t=0} - c_{(C=C)t}\}\{c_{(C=C)t=0}\}^{-1} t^{-1} \ (\text{s}^{-1}) \qquad (2)$$

$$R_{max} = \{c_{(C=C)t1} - c_{(C=C)t2}\}\{t_2 - t_1\}^{-1} (\text{mol m}^{-3}\text{s}^{-1}), \qquad (3)$$

$$R_{max}^m = \{c_{(C=C)t1} - c_{(C=C)t2}\}\{c_{(C=C)t=0}\}^{-1}\{t_2 - t_1\}^{-1} \ (\text{s}^{-1}). \qquad (4)$$

The concentration of the C=C bonds (mol m^{-3}) at time t is $(c_{C=C})_t$, and $(c_{C=C})_{t=0}$ is its concentration at $t = 0$. The time interval used to determine the initial slope was 0–2 s. In general S-shaped plots were found when the change in C=C bond concentration was plotted against t and $R_{ini} < R_{max}$ and $R_{ini}^m < R_{max}^m$. However, when Sb:SnO$_2$ (Sb = 0) particles were used in the starting formulations, no S-shaped plots were found and the rates measured at the beginning of the reaction (R_{ini}, R_{ini}^m) were always the largest rate values obtained. To facilitate the discussion of the results, we still call these rates (R_{ini}, R_{ini}^m). Each experiment was repeated at least three times. The standard deviation $\sqrt{(\sum (x - x_{av})^2/(n - 1))}$ of R from these measurements was taken as error margin. The R_{ini}, R_{max}, R_{ini}^m, and R_{max}^m values determined at 1620 cm^{-1} appeared to be very similar to the ones measured at 1408 cm^{-1}. To facilitate the discussion only the 1620 cm^{-1} data are discussed below.
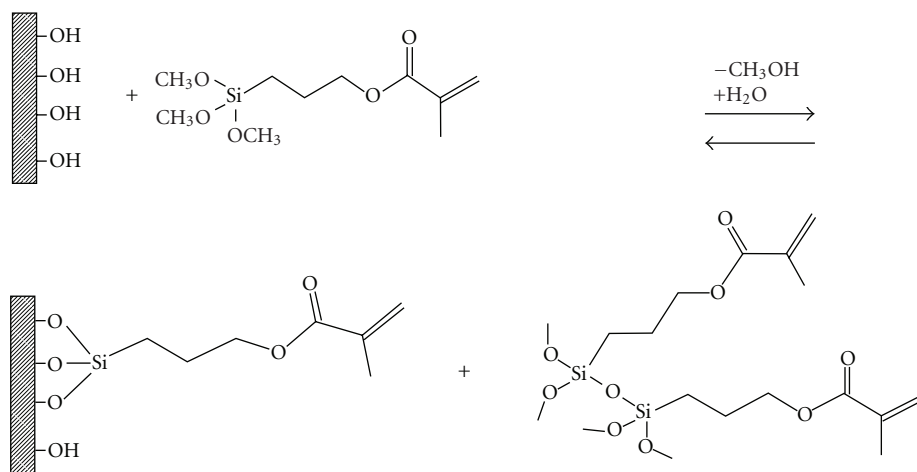
Scheme 2: Schematic presentation of grafting of 3-metacryloxypropyltrimethoxysilane (MPS) to OH-groups of the Sb:SnO$_2$ particle surface and formation of MPS oligomers.

Table 2: Exponential curve fitting of the ratio of σ/σ_0 over time.

Experiment	[Sb:SnO$_2$] vol.%	t_1	t_2	R
UV irradiation	1	424	109	0.99979
UV irradiation	2	471	117	0.99989
UV irradiation	3.8	0	56	0.99974
Vis irradiation	1	2535	—	0.99875
Vis irradiation	2	7330	—	0.94821
Vis irradiation	3.8	1479	—	0.97557

When the surface of the particles was grafted in advance with MPS and the particles were doped with Sb, the photocatalytic conversion of the C=C bonds was complete and a hard, transparent (>98%) crosslinked Sb:SnO$_2$/acrylate film with a low haze (<1%) was obtained. Without MPS grafting the cured Sb:SnO$_2$/acrylate film was inhomogeneous and nontransparent.

2.4. Measurement of the Absorption Spectra of the Sb:SnO$_2$ Dispersions and Photoconduction. The light absorption spectra of aqueous Sb:SnO$_2$ nanoparticle dispersions were recorded with a Shimadzu UV 3102 PC Scanning Spectrophotometer using a rectangular quartz cuvet with a diameter of 1 cm [4]. The photoconduction of the Sb:SnO$_2$/acrylate nanocomposites was investigated on cured acrylate films containing different concentrations of MPS-Sb:SnO$_2$ nanoparticles (Sb doping 13%; MPS/Sb : SnO$_2$ = 0.045 g/g; transparency of the films >98% and haze <1%). These composites were made by light curing of the starting MPS-Sb:SnO$_2$/acrylate formulation in the presence of a standard organic photoinitiator on a polycarbonate substrate (layer thickness after curing about 2.6 μm) [4]. To study the photoconduction the composites were irradiated with UV or visible light. The UV experiments were done in a UVA cube with an Hg UV lamp (dr. Hönle AG, München, Germany) for 60 s with wavelengths 250–400 nm; I_0 = 63 mW cm^{-2} (UV power puck, EIT Inc., Sterling, VA). For the visible

light experiments a fluorescent desk lamp was used (I_0 ≈ 1 mW cm^{-2}; illumination time = 3600 s). The volume conductivity before irradiation σ_0 and after irradiation σ were measured in the dark at room temperature using a four-point probe measurement technique [4]. The change in the ratio of σ/σ_0 over time was analyzed (Origin, Microcal). All UV decays measured were fitted by a bi-exponential function (Table 2). The F-test showed that a single exponential function is insufficient to describe the data adequately at the 5% significance level [22].

All the visible light decays could be fitted best by a monoexponential function (Table 2).

2.5. TEM Measurements. TEM images were obtained with a JEOL 2000FX. Nanocomposite samples of several cured MPS-Sb:SnO2/PEGDA 575 films were prepared by microtome cutting. The samples were approximately 100 nm thick. All showed well-dispersed nanoparticle network structures. One of these images is shown in Figure 1 [4].

3. Results and Discussion

3.1. (MPS)-Sb:SnO$_2$ (Sb ≥ 0%) Nanoparticles as Photoinitiators for (Meth)acrylate Polymerization

3.1.1. Photocatalysis Using Incident Light of 315 nm. Only a limited amount of information is available on the use of
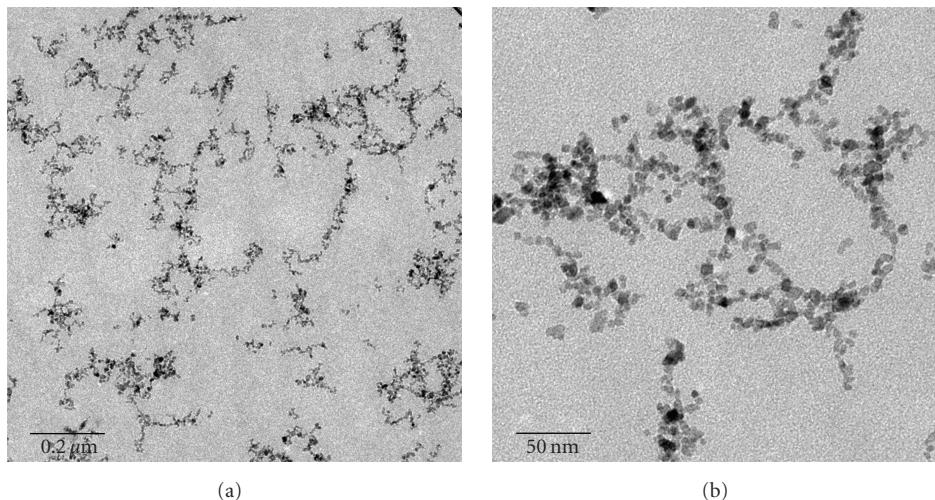
(a)

(b)

FIGURE 1: TEM images of cured semiconductive Sb:SnO$_2$/PEGDA 575 composites at two different amplifications. Sb doping: 2 at.%; layer thickness 100 nm; particle concentration 0.8 vol.%. The particles were grafted before use with MPS (MPS/Sb : SnO$_2$ = 0.045 g/g).

inorganic oxide (nano) particles/layers instead of organic radical photoinitiators to photocatalyse the (meth)acrylate monomer polymerizations [7–9, 23–25]. To our knowledge no information is available about the initiation of (meth)acrylate polymerization by absorption of light by Sb:SnO$_2$ (Sb $\geq$ 0%) present in the form of a (nanoparticle) powder or as a solid layer. Because O$_2$ quenches the radicals formed it is important to perform these reactions in the absence of oxygen [26, 27].

It is well known that the photocatalytic reaction rate of inorganic particles/layers depends on the surface area in contact with the monomer and on the crystallinity of these activators. Hence, in this paper Sb:SnO$_2$ nanoparticles of varying composition but with a similar particle size and crystallinity were used (Table 1). To be certain that these particles are well dispersed in the acrylate monomer before and during irradiation the surfaces of these particles are grafted with MPS. It is well-known that this methacrylate surface modification prevents the agglomeration of the Sb:SnO$_2$ (Sb $\geq$ 0%) nanoparticles in the monomer mixture before and during the curing of the acrylate matrix and that even at low particle concentration particle networks are formed during cure (Figure 1) [1, 4, 28].

As acrylate monomer PEGDA 575 was chosen to limit the influence of the viscosity change during cure on the polymization rate. After cure this layer has a T_g well below room temperature.

The photocatalytic reactions in the Sb:SnO$_2$/PEGDA 575 starting formulations are followed insitu during irradiation under nitrogen. Apart from the Sb:SnO$_2$ particles, no other radical(photo)initiator is present. We found that during irradiation with 315 nm the viscous Sb:SnO$_2$/PEGDA starting formulation is always converted into a hard layer. When no Sb:SnO$_2$ is present a hard cured layer is not obtained under the same processing conditions. This clearly shows that Sb:SnO$_2$ particles photocatalyse the polymerization of the (meth)acrylate formulations.
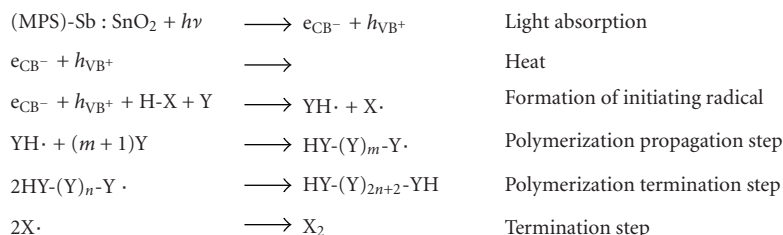
The IR spectrum of a 0.5 vol% MPS-grafted Sb:SnO$_2$/PEGDA 575 formulation before and after irradiation is shown in Figure 2(a). After irradiation the peaks at 1408, 1620, 1637, 1285, 1190, 986 and, 812 cm^{-1} have disappeared. These changes can be explained by the disappearance of the C=C bonds in the acrylate monomer and methacrylate MPS moieties (Table 3) [29]. The same changes as shown in Figure 2(a) are observed when the PEGDA 575 monomer is polymerized by UV radiation in the presence of a standard organic photoinitiator [28]. Hence, Figure 2(a) shows that by direct absorption of UV radiation by the Sb:SnO$_2$ nanoparticles a similar radical polymerization of (meth)acrylate momomers/fragments was observed and that the photocatalytic properties of these particles are such that complete polymerization of the C=C bonds of the (meth)acrylate groups can be realized.

Figure 2(b) shows the IR spectra before and after irradiation of the MPS-grafted Sb:SnO$_2$/PEGDA 575 starting formulation with a much higher particle concentration. Using radiation of the same wavelength and intensity as for Figure 2(a) the acrylate and methacrylate bands at 1408, 1620, 1637, 1285, 1190, 986 and 812 cm^{-1} disappeared in Figure 2(b) in a similar way. Moreover, Figure 2(b) also shows an overall broad IR absorbance before UV irradiation which was enhanced after UV irradiation. This broad IR absorbance, known as plasmon band, is due to the reflection of the electric field of the incident IR radiation by the combined oscillations of the electrons in the conduction band of the semiconducting Sb:SnO$_2$ nanoparticles [17, 30–34]. The intensity of this broad plasmon band depends on the concentration of the Sb:SnO$_2$ nanoparticles and could only be observed at higher particle concentrations (Figure 2(b)). This increase in absorption after irradiation can be explained by the increase in the number of electrons in the conduction band. The distance between the valence band and conduction band of Sb:SnO$_2$ (Sb $\geq$ 0) particles is about 3.6 eV [17, 18], which corresponds to a wavelength

TABLE 3: Assignment of the characteristic FT-IR bands of PEGDA 575 and MPS [29].

Vibration	PEGDA	MPS	Vibration	PEGDA	MPS
C=O stretch	$1721\ cm^{-1}$	$1717\ cm^{-1}$	C–O stretch	$1298\ cm^{-1}$	$1325\ cm^{-1}$
C=C stretch	$1637\ cm^{-1}$	$1637\ cm^{-1}$	C–O stretch	$1270\ cm^{-1}$	$1300\ cm^{-1}$
C=C stretch	$1620\ cm^{-1}$	—	C–O stretch	$1190\ cm^{-1}$	$1187\ cm^{-1}$
=CH_2 bend	$1408\ cm^{-1}$	—	=CH wag	$986\ cm^{-1}$	—
=CH_2 twist	$810\ cm^{-1}$	$814\ cm^{-1}$	—	—	—
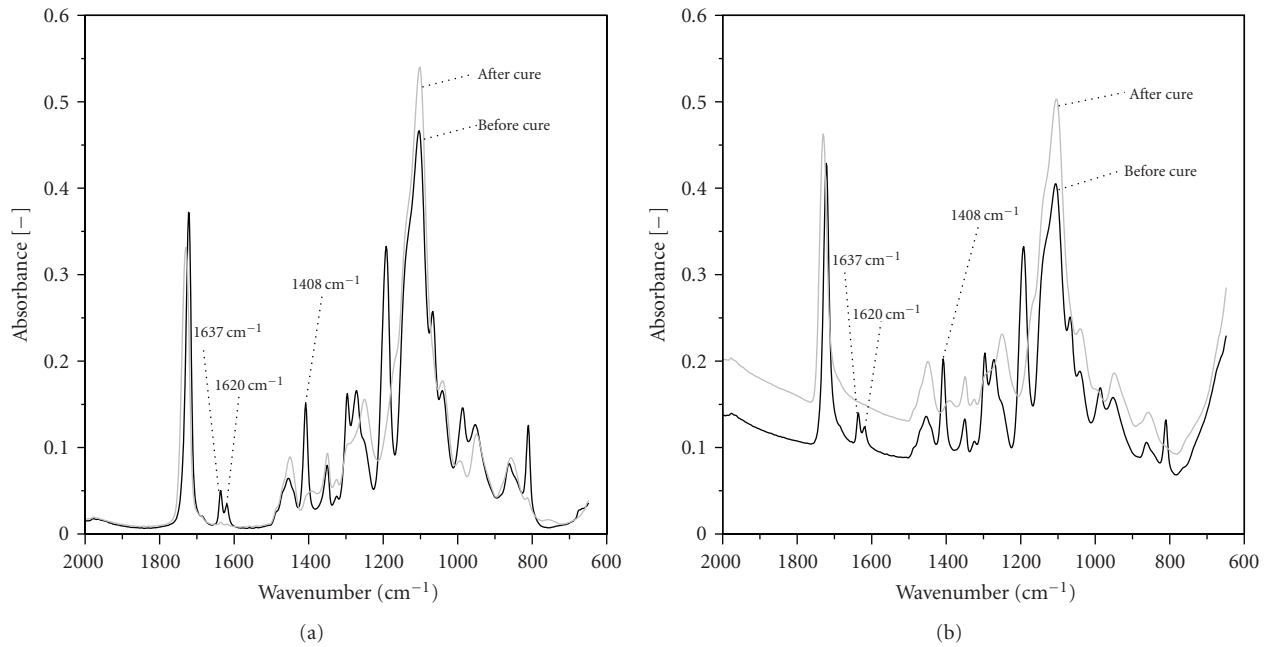
FIGURE 2: ATR FT-IR spectra of Sb:SnO$_2$/PEGDA starting formulations before and after irradiation with 315 nm light. Sb = 13%; MPS/Sb:SnO$_2$ = 0.08 g/g. (a) 0.5 vol% Sb:SnO$_2$ particles; (b) 10 vol% Sb:SnO$_2$ particles.
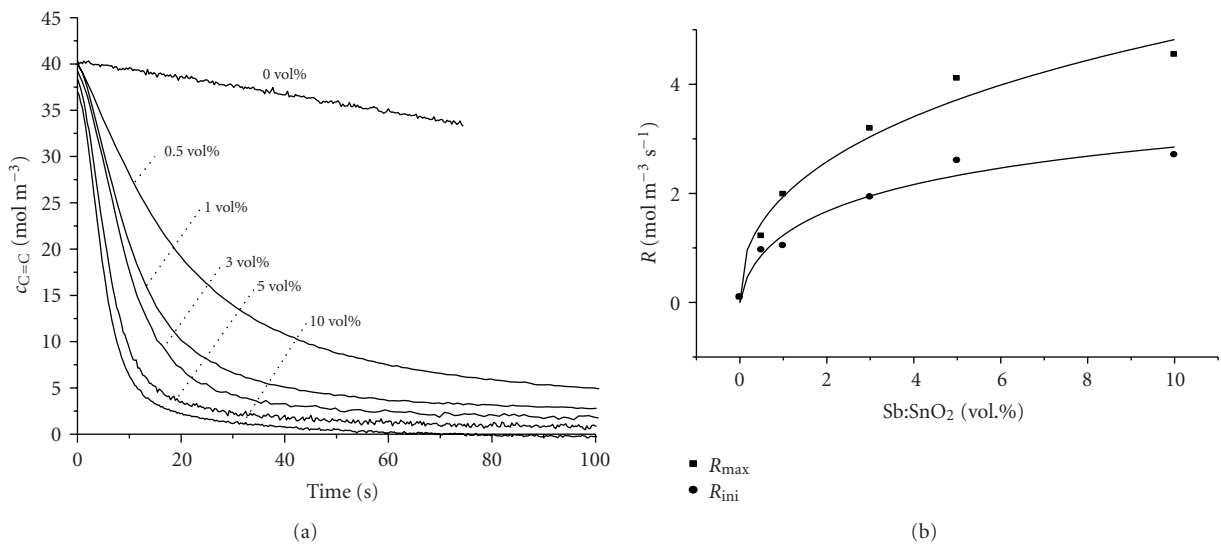
FIGURE 3: Dependency of the photocatalysed C=C bond conversion on Sb:SnO$_2$concentration measured at $1637\ cm^{-1}$ (13% Sb; MPS/Sb:SnO$_2$ = 0.08 g/g). (a) The change in the (meth)acrylate C=C bond concentration during irradiation. (b) R_{max}^{1637} and R_{ini}^{1637} determined from the slopes in Figure 3(a) (points; (1)).] The solid lines represent the polymerization rate calculated with (5) using for K_{max}^{1637}:$2.20 \times 10^{-4}\ m^{3/2}\,s^{-1/2}\,J^{-1/2}$ and $K_{ini}^{1637} = 1.44 \times 10^{-4}\ m^{3/2}s^{-1/2}J^{-1/2}$.

$$(MPS)\text{-}Sb : SnO_2 + h\nu \longrightarrow e_{CB^-} + h_{VB^+} \qquad \text{Light absorption}$$

$$e_{CB^-} + h_{VB^+} \longrightarrow \qquad\qquad\qquad \text{Heat}$$

$$e_{CB^-} + h_{VB^+} + H\text{-}X + Y \longrightarrow YH\cdot + X\cdot \qquad \text{Formation of initiating radical}$$

$$YH\cdot + (m+1)Y \longrightarrow HY\text{-}(Y)_m\text{-}Y\cdot \qquad \text{Polymerization propagation step}$$

$$2HY\text{-}(Y)_n\text{-}Y\cdot \longrightarrow HY\text{-}(Y)_{2n+2}\text{-}YH \qquad \text{Polymerization termination step}$$

$$2X\cdot \longrightarrow X_2 \qquad\qquad\qquad\qquad \text{Termination step}$$

SCHEME 3: Mechanism for radical polymerization of the (meth)acrylate C=C double bonds initiated by the absorption of light by these Sb:SnO₂ particles. (MPS)-Sb:SnO₂: particles grafted or not grafted with MPS, Y is PEGDA 575 monomer, grafted MPS and/or MPS oligomer (Scheme 2). H-X is a hydrogen donor.
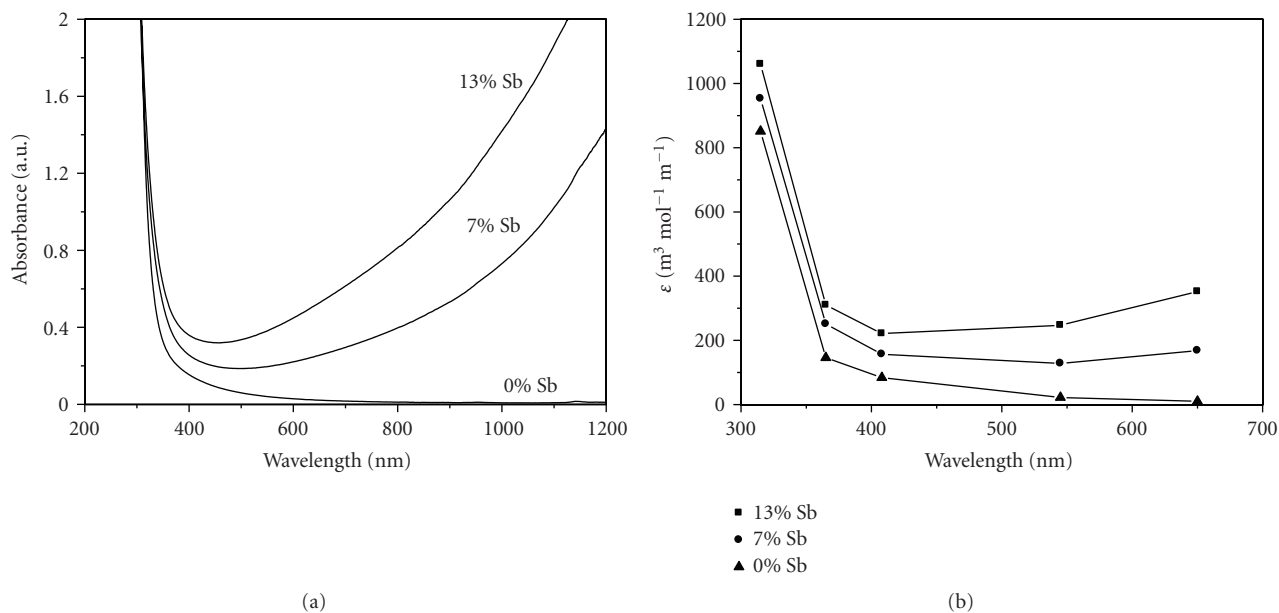

(a)

(b)

FIGURE 4: (a) UV/Vis absorbance spectra of ungrafted Sb:SnO₂ (Sb ≥ 0) in aqueous dispersion (0.23 wt%). (b) Molar extinction coefficients, ε of Sb:SnO₂ particles at different wavelengths, not corrected for the Plasmon band contribution.

of about 340 nm. Hence, during irradiation with 315 nm the number of electrons in the conduction band as well as the reflection of IR light increases. Similar increases in intensity were observed when starting formulations with other Sb:SnO₂ (Sb ≥ 2%) particles where use Sb:SnO₂ (Sb = 0%) particles have a plasmon peak which can be measured with our unit and we observed that after irradiation with 315 nm not only the peak position, but also the onset of the plasmon band shifted to higher wave numbers in the IR spectrum. This confirms that indeed the number of electrons in the conduction band increased during irradiation [35].

We also observed that after switching of the irradiation these enhanced plasmon band absorptions decreased only slowly over time. This shows that the rate of recombination of the excited electrons and holes is slow in these cured MPS-Sb:SnO₂/acrylate layers (see also later on).

3.1.2. Influence of Sb:SnO₂ Particle Concentration on Curing Rate. The influence of the Sb:SnO₂ particle concentration on the rate of the polymerization of the C=C bonds of the (meth)acrylate monomers/fragments is shown in Figure 3.

When the Sb:SnO₂ particle concentration is increased, the rate of C=C bond disappearance over time enhances. Hence, the photocatalytic C=C bond polymerization is dependent on the concentration of the Sb:SnO₂ particles present in the starting formulation. For all our formulations the polymerization rate strongly decreases in the presence of oxygen. Hence, a radical mechanism is likely to occur. Figure 3(a) suggests that at the end of the reaction both types of C=C bonds have disappeared. However, a comparison of Figures 2(a) with 2(b) suggests that the contribution of the MPS is too small to be detected. Stronger evidence that indeed both C=C bonds react chemically and form part of the matrix polymer after irradiation will be presented later on. Figure 3(a) also shows that a very slow acrylate monomer polymerization takes place when Sb:SnO₂ particles are not present. This can be explained by the direct absorption of light by the acrylate monomer. Such a very slow rate of self-polymerization with light of 315 nm of the (meth)acrylate monomer in absence of an organic photoinitiator or Sb:SnO₂ particles was observed earlier [28]. We neglect this small contribution to the rate of polymerization of the acrylate monomer in the discussions below.

The bandgap of the Sb:SnO$_2$ particles is about 3.6 eV and the absorption of a light quantum of 315 nm will result in the excitation of an electron from the valence band directly into the conduction band and in the formation of a hole in the valence band [17]. In principle, both the electron in the conduction band (e_{cb}^-) and the hole in the valence band (h_{vb}^+) can initiate (meth)acrylate C=C bond polymerization in the presence of a hydrogen donor. It has been shown for several other semiconductor inorganic (nano)particles that under UV irradiation these particles can initiate free radical polymerization of a methacrylate monomer in the presence of a hydrogen donating component/solvent [7, 9, 36]. Based on the reaction schemes in these publications the photocatalytic polymerization of the C=C bonds in the MPS-Sb:SnO$_2$/acrylate starting formulations may be explained as shown in Scheme 3.

In the presence of a hydrogen donor (H-X), the activated electron in the conduction band and the hole in the valence band react and a (meth)acrylate radical (YH·) is formed. This radical will start the polymerization propagation reaction of the C=C bonds. As will be shown later, the most likely termination reaction is the addition of two polymer fragments with acrylate radical end groups. The YH· radical formed may contain a chemically connected Sb:SnO$_2$ particle. Essential in this mechanism is also the transfer of a hydrogen and a reaction with the hole h_{VB^+}. In our formulations such a hydrogen source may be a hydrogen-containing surface group, such as –OH, NH$_3$ and/or grafted MPS. Also the presence of metal ions, such as Sb(V) may influence this transfer reaction. We will show below that Scheme 3 can be used to quantify the C=C bond polymerization rates of our formulations and that detailed information can be obtained for Φ, k_p and k_t (see (6)) when the nanoparticles are grafted with MPS and doped with Sb.

For radical (meth)acrylate polymerization using nanoparticles as photocatalysts, a basic expression for the propagating polymerization rate R_p (mol m^{-3} s^{-1}) was proposed (see (5)) [7, 9, 36]. In this relation the decrease of C=C bond concentration c_M (mol m^{-3}) in time t [s] is a function of the propagating and terminating reaction rate constants k_p and k_t (m^3 mol^{-1} s^{-1}), respectively, the quantum yield for the formation of the initiating radical Φ (mol J^{-1}), the incident radiation intensity I_0 (J m^{-2} s^{-1}), the molar extinction coefficient of the absorbing Sb:SnO$_2$ particles ε (m^3 mol^{-1} m^{-1}), the particle concentration $c_{particle}$ (mol m^{-3}) and the thickness of the irradiated film d (m). A relative quantum efficiency K is defined [9]. A very similar approach was used to quantify the UV-photocatalyzed polymerization propagation rate of (meth)acrylate C=C bonds initiated by an organic photoinitiator [37, 38].

$$R_p = -\frac{dc_M}{dt} = k_p c_M \sqrt{\frac{\Phi I_0 \left(1 - 10^{-\varepsilon c_{particle} d}\right)}{d k_t}}$$

$$= K c_M \sqrt{\frac{I_0 \left(1 - 10^{-\varepsilon c_{particle} d}\right)}{d}}, \tag{5}$$

$$K = k_p \sqrt{\frac{\Phi}{k_t}} \left[m^{3/2} s^{-1/2} J^{-1/2}\right]. \tag{6}$$

We calculated the R_{max}^{1637} values from the data of Figure 3(a) for each Sb:SnO$_2$ concentration by combining (5) and (2) (Figure 3(b)). We assumed that the R_{max}^{1637} shown in Figure 3(b) is equal to the R_p of (5) and that k_p, k_t, and Φ are independent of the particle concentration we determined K_{max}^{1637} from the data in Figure 3(b) using for ε the values determined from the UV absorbance spectra of the Sb:SnO$_2$ nanoparticle dispersions (Figure 4), the measured values for I_0 and d. A good relation between the calculated and experimentally determined R_{max}^{1637} is obtained with K_{max}^{1637} = 2.20 × 10^{-4} (m$^{3/2}$ s$^{-1/2}$ J$^{-1/2}$) (Figure 3(b)). The good fit in Figure 3(b) supports the proposed reaction mechanism in Scheme 3 and the use of (5) for the photocatalytically initiated (meth)acrylate polymerization by the Sb:SnO$_2$ nanoparticles. We also followed the absorption over time at 1620 cm^{-1} and calculated the R_{max}^{1620} values for these absorptions (data not shown). Both R_{max} values appear to be very similar. At 1620 cm^{-1} only the C=C bonds of the acrylate monomer absorb, whereas at 1637 cm^{-1} both the C=C bonds of the methacrylate (MPS) moieties and the C=C bonds of the acrylate monomer absorb. This suggests that the R_{max} values shown in Figure 3(b) are the propagation polymerization rates of the acrylate C=C bonds. Further evidence for this will be shown later on. For all the formulations studied in Figure 3 the initial rate of C=C disappearance R_{ini} is always slower than R_{max}. When we used the same approach to compare the experimentally determined and the calculated R_{ini}^{1637} we obtained the best fit with K_{ini} = 1.44 × 10^{-4} m$^{3/2}$ s$^{-1/2}$ J$^{-1/2}$ (Figure 3(b)). The reason why the K_{ini}^{1637} is smaller than K_{max}^{1637} will be explained in the next section.

3.1.3. Influence of MPS Grafting of Sb:SnO$_2$ (Sb = 7%) Particles. Sb:SnO$_2$ nanoparticles without a specific surface modification are agglomerated in slightly polar organic media, such as acrylate monomers [1, 4, 28]. The amount of agglomeration depends strongly on the dispersion method used. This agglomeration will lower the amount of surface contact between the particles and the polymerizable monomer and influence the transfer of activated electrons from the particles to polymerizable C=C bonds. Hence, for obtaining quantitative data in our photocatalytic experiments, it is very important to use nonagglomerated Sb:SnO$_2$ nanoparticles in the PEGDA formulations. We have shown before that well-dispersed Sb:SnO$_2$ particle PEGDA dispersions can be made, when the surfaces of these particles are grafted with the methacrylate silane coupling agent MPS (Figure 1) [1, 4, 21, 28]. Therefore, in general, MPS grafted Sb:SnO$_2$ particles are used in this paper.

Grafting a nanoparticle dispersion with MPS introduces polymerizable methacrylate C=C bonds in the starting Sb:SnO$_2$/PEGDA formulations. These bonds can be present as dispersed MPS oligomers and/or MPS moieties grafted on the surface of the particles (Scheme 2) [21]. MPS oligomers

cannot be separated from the grafted MPS particles in dispersion without lowering the dispersion quality in the acrylate monomer [28]. It is known that the presence of methacrylate C=C bonds influences the acrylate radical polymerization reaction [39, 40]. Hence, for a quantitative comparison it is essential to know both MPS concentrations. These amounts were determined by combining ultracentrifuge separating methods with elemental and BET surface analyses (Figure 5). The good fit between the solid lines and square points in Figure 5 shows that the total amount of MPS added to the grafting Sb:SnO$_2$ dispersion is still present at the end of the reaction. For a MPS/Sb : SnO$_2$ ≤ 0.08 g/g all the MPS added has been grafted on the Sb:SnO$_2$ surface and when MPS/Sb : SnO$_2$ > 0.08 is used the grafted MPS amount hardly increases further. Almost all the additional MPS is converted into MPS oligomer. Miller and Ishida have calculated the amount of grafted MPS needed to cover the surface with a monolayer of parallel-oriented MPS [41]. Their results suggest that for MPS/Sb : SnO$_2$ ≥ 0.08 g/g an (almost) complete monolayer of grafted MPS is always present with an orientation parallel to the Sb:SnO$_2$ particle surface. That indeed such a MPS orientation is present on the surfaces of our grafted particles is confirmed by the shift in position of the carbonyl absorptions in the FT-IR spectra (for instance, Figure 2) as was explained before in [21]. NH$_3$ groups are also present on the surface of the Sb:SnO$_2$ particles [4]. The amount increases with an incease in Sb doping [4]. These NH$_3$ amounts are not changed after MPS grafting. Our calculations suggest that the observed relation between NH$_3$ and Sb amount explain the lowering in MPS plateau level when the amount of Sb doping becomes larger.

The amount of MPS grafted on Sb:SnO$_2$ particles was determined earlier with FT-IR. A somewhat lower level of MPS grafting was reported [1, 15, 28]. We used also this method and found that the FT-IR method results into a larger error of measurement.

Figure 6(a) shows that the amount of MPS present influences the photocatalytic C=C bond polymerization. These data suggest that the influence of grafted MPS is much stronger than that of MPS oligomer. Moreover, only when the Sb:SnO$_2$ (Sb > 0%) nanoparticle is grafted with MPS an S-shape relation is found between the decrease in the C=C bond absorption and the reaction time. Figure 6(a) also suggests that the initial C=C bond polymerization rate is much faster when these particles are not grafted with MPS. Apparently grafted MPS slows down the C=C bond polymerization. When the Sb:SnO$_2$ surface is not grafted with MPS the particles are always already agglomerated before irradiation. During irradiation we observed that this agglomeration further increases, becomes visible by the naked eye and that the C=C bonds are only partly converted at the end of the reaction and the cured films are no longer transparent. Hence, results for the nongrafted Sb:SnO$_2$/PEGDA mixtures can only be used in a qualitative way.

For a quantitative comparison of the C=C double bond conversions of Figure 6(a) we have to take into account the variation in the C=C bond concentration at time

$t = 0$ ($c_{(C=C)t=0}$). by using (2) and (4). That means that for R_{ini}^m and R_{max}^m (5) has to be changed into (7) and (8).

$$R_{ini}^m = K_{ini}\{c_{(C=C)t=0} - c_{(C=C)t}\}\{c_{(C=C)t=0}\}^{-1}$$
$$\times \{I_0\left(1 - 10^{-\varepsilon.c particle.d}\right)d^{-1}\}^{1/2} \tag{7}$$

$$R_{max}^m = K_{max}\{c_{(C=C)t1} - c_{(C=C)t2}\}\{c_{(C=C)t=a}\}^{-1}$$
$$\times \{I_0\left(1 - 10^{-\varepsilon.c particle.d}\right)d^{-1}\}^{1/2} \tag{8}$$

$$K_{ini/max} = k_{p(ini/max)}\{\Phi\left(k_{t(ini/max)}\right)^{-1}\}^{1/2}. \tag{9}$$

The $c_{(C=C)t=a}$ is the C=C bond concentration averaged over time period t_2-t_1.

For the formulations presented in Figure 6(b) the R_{max}^m values were measured at 1637 and 1620 cm^{-1}. Within the error of measurement these R_{max}^m values appeared to be equal. Hence, the R_{max}^m values presented in Figure 6(b) are the polymerization rate between a polymer fragment with an acrylate radical end group and an acrylate monomer [28, 29]. Figure 6(b) also shows that the R_{max}^m values decrease, when the amount of MPS moieties increases, and at MPS/Sb : SnO$_2$ = 0.2 the R_{max}^m is lowered by 50%. For formulations for which particles grafted with MPS/Sb : SnO$_2$ = 0.2 are used the $c_{(C=C)t=0}$ is less than 10 mol% larger than for formulations which contained particles not grafted with MPS (MPS/Sb : SnO$_2$ = 0). Hence, the decrease in R_{max}^m shown in Figure 6(b) is too large to attribute it to the increase in $c_{(C=C)t=0}$ only. That means that also the K_{max} values decrease when the MPS/Sb:SnO$_2$ ratio is increased. Because $k_{t(max)}$ and $k_{p(max)}$ are expected to be independent of the MPS/Sb:SnO$_2$ ratio we conclude that Φ becomes smaller when the grafted amount of MPS increases in the starting mixture. After correcting the R_{max}^m for the variable $c_{(C=C)t=0}$ it appears that MPS oligomer hardly influences R_{max}^m. Therefore Φ depends on the amount of grafted MPS, and grafted MPS slows down the transfer of an electron from the conduction band to the C=C acrylate monomer, possibly because of the direct formation of a grafted MPS radical on the particle surface.

Posthumus studied the rate of C=C homopolymerization of PEGDA 575, MPS monomer, and of PEGDA 575/MPS monomer mixtures in detail with IR spectroscopy at 1637 cm^{-1} (Figure 7) [28]. These radical polymerizations were initiated by a standard organic radical photoinitiator and the rates of the polymerizations were measured using a very similar approach and setup. Figure 7 shows that the homopolymerization rates of an MPS monomer are much smaller than thoses of a PEGDA 575 monomer and that for MPS/PEGDA 575 monomer mixtures the initial and maximum polymerization rates decrease when the relative amount of MPS is increased [21]. Moreover, for MPS/PEGDA monomer mixtures an S-shape relation is found. Hence, the influence of MPS oligomers and/or grafted MPS on the C=C bond polymerization rates and on the S-shape of the curves in Figure 6(a) can be attributed to the presence of MPS in these MPS-Sb:SnO$_2$/PEGDA

starting formulations. Posthumus also reported that the rate of disappearance for MPS/PEGDA monomer mixtures at the earlier stage of the reaction was much faster for the methacrylate C=C bond of the MPS than for the acrylate C=C bond of PEGDA monomer, even when the methacrylate concentration was much lower. This difference in C=C bond radical polymerization rate occurs because the initial rate is far more determined by the propagating methacrylate radical structure than by the much faster reactivity of the acrylate [28, 39, 40]. We also observe these methacrylate/acrylate mixture effects at the initial stage of the C=C polymerization (Figure 6(b)). The R_{ini}^{m} strongly decreases when the amount of grafted MPS increase. The decrease is far too large to be explained by differences in $c_{(C=C)t=0}$. Moreover the R_{ini}^{m} (MPS/Sb : SnO_2 > 0) at $1620 \, cm^{-1}$ is always lower than the R_{ini}^{m} at $1637 \, cm^{-1}$ (Figure 6(b)), and the difference between these two values becomes larger when the MPS C=C double bonds increase further. Hence, at the initial stage of the reaction methacrylate C=C bonds prefer also to react with a methacrylate radical end group in our MPS-Sb:SnO_2/PEGDA formulations.

Figure 6(b) showns that when Sb:SnO_2 (Sb = 7%) nanoparticles are grafted with MPS the R_{ini}^{m} at $1620 \, cm^{-1}$ is considerable lower than R_{max}^{m} at $1620 \, cm^{-1}$. Apparently R_{ini}^{m} represents the reaction of an acrylate C=C double bond. Figure 6(b) also shows that this C=C polymerization rate is the largest when the particle surface is not grafted with MPS. Hence, grafted MPS influences the polymerization rate in two ways. First of all is by lowering Φ. Secondly, the grafted MPS lowers the $k_{p(ini)}(k_{t(ini)})^{-1/2}$ ratio of (9). This may be explained by the formation of a grafted MPS radical on a particle surface first. This conclusion is further supported by the lower values of R_{ini} in respect to R_{max} in Figure 3.

The C=C bond absorptions of the starting MPS-Sb:SnO_2/PEGDA formulations disappear at the end of the reaction. Hence, all the C=C double bonds are polymerized during curing, and the Sb:SnO_2 particles and MPS oligomers are chemically connected to the polymer matrix. This will influence the nanoparticle network structure and introduce crosslinks in the polymer matrix of the cured MPS-Sb:SnO_2/acrylate composites and explain the hard layers obtained at the end of the reaction.

3.1.4. Influence of Sb Doping. In this section the influence of Sb doping (0%–13%) on the photocatalytic conversions of the C=C bonds over time measured at 1637 and $1620 \, cm^{-1}$ and their corresponding R_{ini}^{m} and R_{max}^{m} values is discussed (Figures 8(a) and 8(b)).

Figure 8(a) shows that for Sb:SnO_2 particles with 2% ≤ Sb ≤ 13%, C=C conversion percentages at 1637 and $1620 \, cm^{-1}$ are very similar at any moment in time. After correcting the R_{max}^{m} values of Figure 8(b) for the small differences in extinction coefficient (Figure 4), it appears that the K_{max}^{m} and the corresponding k_p and the k_t values are almost equal and that therefore $\Phi^{Sb\geq2\%}$ at 315 nm is independent of the amount of Sb doping. In Figure 8(b) it is also shown that the R_{max}^{m} values measured at $1637 \, cm^{-1}$ are equal to those measured at $1620 \, cm^{-1}$. Hence, these
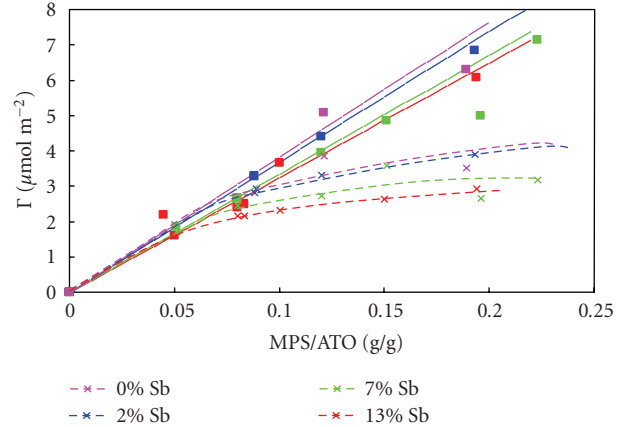

FIGURE 5: Amount of MPS grafted on the surface of the Sb:SnO_2 (ATO) nanoparticles (crossings) as a function of the MPS/Sb:SnO_2 ratio used in the grafting reaction. The solid lines and squares are the total amount of MPS added to the starting grafting mixture. The crossings are the grafted MPS amounts on the Sb:SnO_2 particles.

R_{max}^{m} values are the rates of the propagation step of the polymerization between a polymer fragment with an acrylate end group and an acrylate monomer. As is observed and discussed earlier the R_{ini}^{m} values depend on the IR absorption band used. The R_{ini}^{m} values measured at $1637 \, cm^{-1}$ are always about 30% larger than those measured at $1620 \, cm^{-1}$ for Sb:SnO_2 particles (2% ≤ Sb ≤ 13%). This shows that at the initial stage of the curing reaction there is a preference for a reaction between a polymer with a methacrylate radical end group and a methacrylate C=C bond.

Figure 8(a) suggests that when the nanoparticles are not doped with Sb the % conversion of the C=C bonds over time is similar to those observed for Sb-doped particles. However, Figure 8(b) shows that for nondoped particles the R_{ini}^{m} measured at $1637 \, cm^{-1}$ and the R_{ini}^{m} measured at $1620 \, cm^{-1}$ are 50% larger than for the doped particles, and therefore the initial $\phi^{Sb=0}$ seems to be about twice as large as the initial $\phi^{Sb\geq2\%}$. Apparently Sb doping lowers ϕ by trapping (part of) the activated electrons from the conduction band. When the Sb:SnO_2 particles are non-doped with Sb, the energy needed for the formation of oxygen vacancies is low and these are likely to be present in the crystals without Sb doping [42] resulting in deep impurity (donor) energy levels of about 0.14 eV below the conduction band minimum in these particles, which are broadened as the concentration of impurities increases [43]. Hence, much higher $\Phi^{Sb=0}$ may be also partly explained by the influence of the energy levels due to oxygen vacancies on the C=C polymerization rate. Photoluminescence experiments on SnO_2 nano at 300 nm confirm that oxygen vacancies in the bulk and O^{2-} at the surface can be efficient hole scavengers [44]. Moreover, these oxygen vacancies destabilize often these particles [42, 43]. We found that in the dark the non-doped particles are stable in the formulations used here. However, during irradiation, photocatalyzed unwanted site reactions occur, which are likely to be activated by the oxygen vacancies and which become more apparent at a later stage of the polymerization.
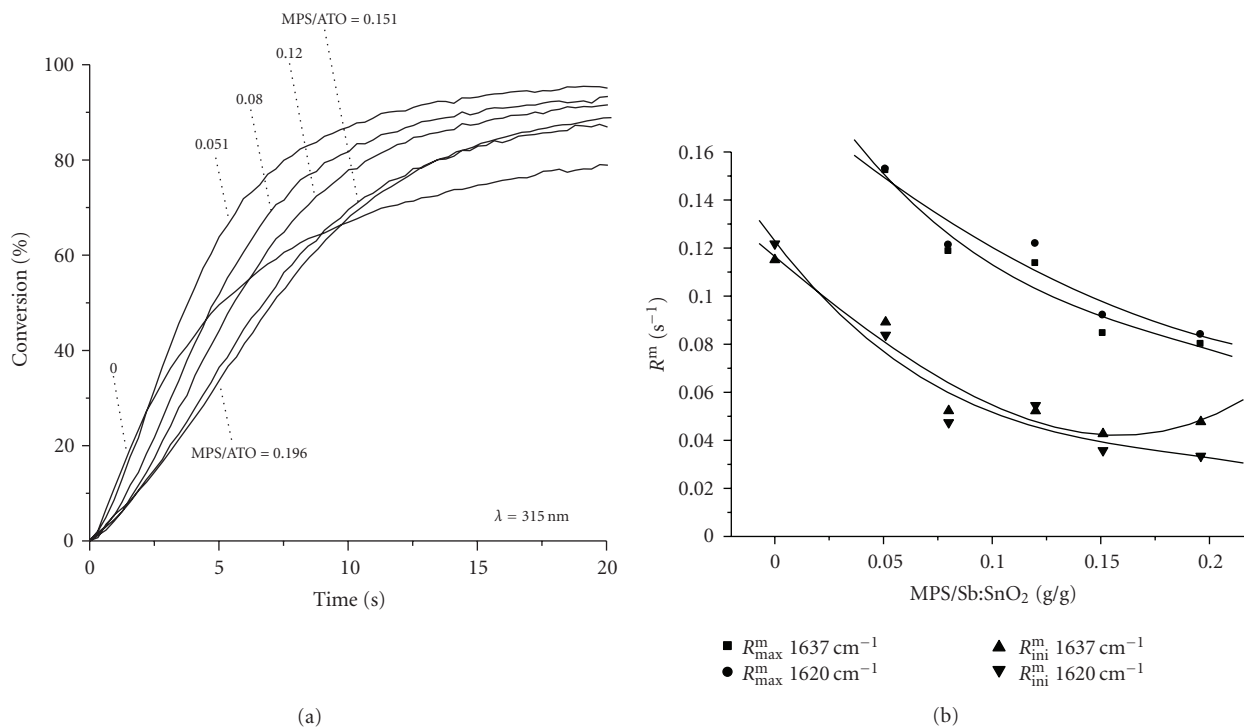
(a)

(b)

FIGURE 6: Dependency of the photocatalysed C=C bond conversion on the MPS amount present in the Sb:SnO$_2$/PEGDA formulations (10 vol.% Sb:SnO$_2$, Sb = 7% Sb; MPS/Sb : SnO$_2$ = 0.08 g/g). (a) Relative conversions of C=C bonds measured at 1637 cm^{-1}. (b) R_{max}^m, R_{ini}^m as a function of MPS/Sb:SnO$_2$ ratios measured at 1637 and 1620 cm^{-1}.
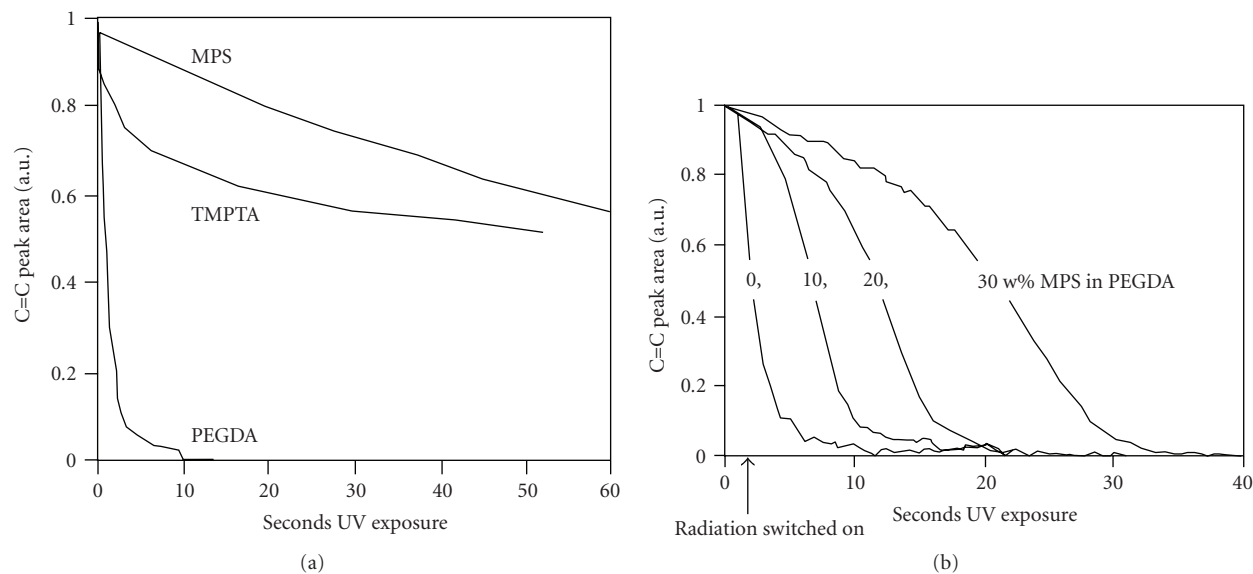

(a)

(b)

FIGURE 7: UV radical polymerization of MPS and PEGDA 575 monomers photocatalysed by 2-hydroxy-2-methyl propiophenone under nitrogen followed by real-time FTIR (at 1637 cm^{-1}) [28]. (a) Homopolymerizations of the (meth)acrylate monomers.; (b) copolymerizations of the (meth)acrylate monomers.

The products of these unwanted site reactions may also enhance $\Phi^{Sb=0}$. A similar but smaller increase in % conversion of C=C bonds for non-MPS grafted Sb:SnO$_2$ (Sb = 0%) particles at the initial stage of the reaction was shown in Figure 6(a). Here, apart from the influence of additional agglomeration of the particles before and during the reaction on the rate of the polymerization reaction, these unwanted

site reactions seem to become dominant and block later on almost completely the conversion of the C=C bonds.

In our Sb:SnO$_2$/PEGDA 575 formulations always highly crystalline Sb:SnO$_2$ particles are used which have a similar particle diameter size (Table 1). They are n-type semiconductor particles with a band gap of about 3.6–3.8 eV and a Fermi level of about 0.35–0.5 eV below the conduction band
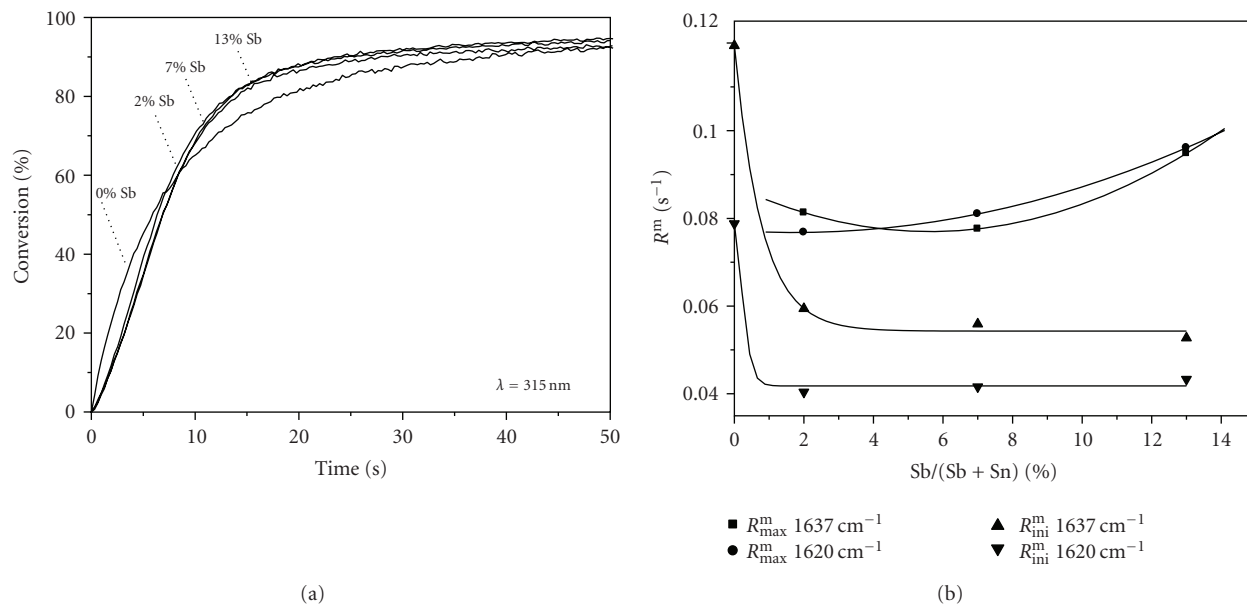
(a)

(b)

FIGURE 8: Dependency of the photocatalysed C=C bond conversion on the Sb doping level of the Sb:SnO$_2$ particles (10 vol.% Sb:SnO$_2$, 0% ≤ Sb ≤ 13%; MPS/Sb : SnO$_2$ = 0.19 g/g). (a) Relative C=C bond conversions over time measured at 1637 cm^{-1}. (b) The R_{max}^m and R_{ini}^m measured as a function of Sb/(Sb + Sn) at 1637 and 1620 cm^{-1} different wave numbers.

[17, 18]. By enlarging the amount of Sb doping not only the amounts of Sb(V) increases, but also Sb(III) ions are present in the particles with Sb ≥ 7% (Table 1) [4]. The Sb(V) ions are mainly present in the bulk, and Sb(V) energy levels are expected to be about 0.03 eV to 0.15 eV below the minimum of the conduction band [45, 46]. That $\phi^{Sb \geq 2\%}$ is almost independent of the amounts of Sb doping may be explained by the assumption that at Sb(V) levels trap the activated electrons from the conduction band and that at Sb = 2% the amount of Sb (V) energy levels are already present in quite large amounts. The influence of Sb(III) ions, mainly present at the surface of the particles, seems to be limited [4].

We were initially amazed that Sb doping lowers the quantum yield for the formation of the initiating radical for the C=C bond polymerization, but recent literature shows that not all doped ions in, for instance, TiO$_2$, stimulate electron-induced photocatalysis and that doped metal ions can serve as sites for electron-hole recombination and lower actually the quantum yields [47, 48]. The results presented above makes it likely that the transfer rate of the activated electron to grafted MPS is partly retarded by Sb(V) when MPS grafted Sb:SnO$_2$ (Sb > 0) particles are used in the formulations.

The results discussed above suggest that variations in the bulk and surface compositions of Sb:SnO$_2$ particles (2% ≤ Sb ≤ 13%), apart from MPS and Sb(V) doping differences, seem to have a limited influence on the photocatalyzed C=C polymerization when incident radiation of 315 nm is used (for instance, the amount of N(III) in the bulk and the NH$_3$ groups at the surface) (Table 1). N-doping enhances the photocatalytic properties of TiO$_2$ and based on the values reported for TiO$_2$ doped with iron the N(III)

energy levels in the Sb:SnO$_2$ particles are expected at 0.7 eV above the maximum of the valence bond [49]. Moreover, it has been shown that specific surface groups on inorganic nanoparticles may enhance the photocatalysis considerably and may suppress the rate of electron-hole recombination [8]. Other specific surface groups may also enhance the photocatalytic properties of our particles. Why the N(III) in the bulk and NH$_3$ and Sb(III) ions at the surface of the particles do not influence the rate of the photocatalysed C=C bond polymerization reactions is unclear at this moment.

Many articles are published about Sb:SnO$_2$ materials (for instance, [3, 49, 50]). At least for the preparation of part of these materials Sb:SnO$_2$ dispersions were used similar to the ones described above. Why the photocatalytic properties of these materials were never mentioned before is unclear at this moment.

3.2. Photoconduction in Cross-Linked Semiconductive MPS-Sb:SnO$_2$/Acrylate Nanocomposites.

The addition of MPS-Sb:SnO$_2$ nanoparticles (Sb ≥ 2%) enhances the conductivity of an isolating acrylate matrix when the filler concentrations are above the percolation threshold ϕ_c [1, 4–6]. We showed that these cured composites have a very low ϕ_c (0.3 vol. %). The increase in the conductivity is caused by the formation of a continuous Sb:SnO$_2$ particle network structure through the acrylate matrix during curing. Scouting experiments showed that the volume conductivity σ of these films increased with respect to the volume conductivity in the dark σ_0, when they were irradiated with UV or visible light. This increase in conductivity depends strongly on the light intensity used and the amount of Sb:SnO$_2$ particles (Sb ≥ 2%) present. In this paper the photoconduction experiments on films prepared from very similar Sb:SnO$_2$ acrylate dispersions
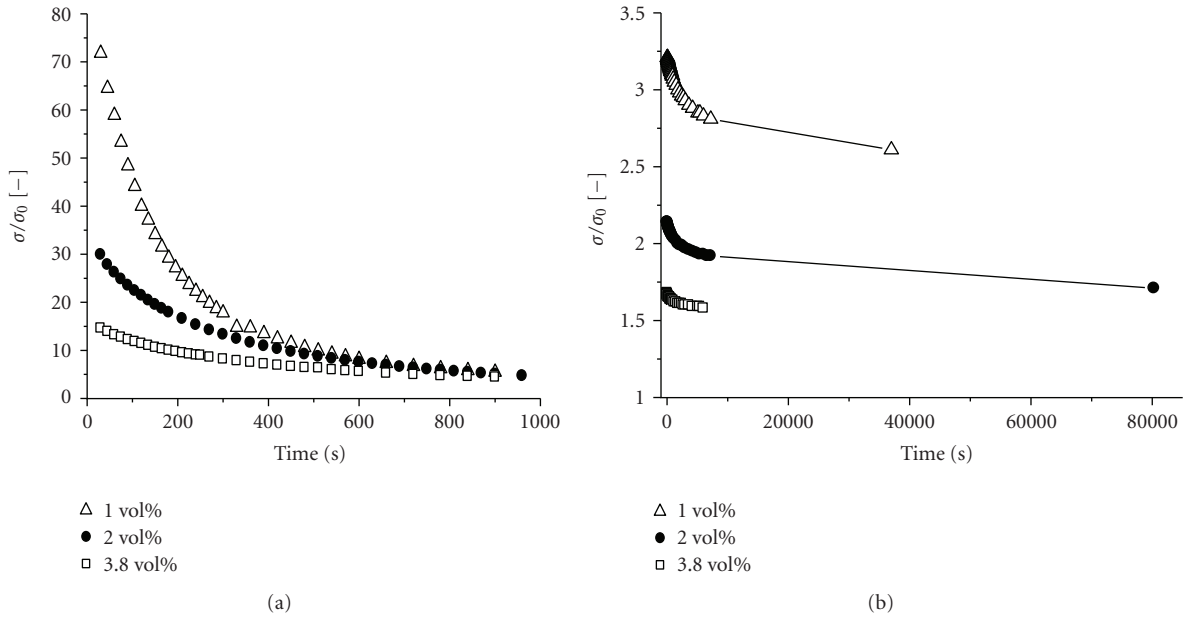
(a)

(b)

FIGURE 9: Photoconduction of cured MPS-Sb:SnO$_2$/acrylate composites at different Sb:SnO2 concentrations (Sb = 13%; MPS/Sb : SnO$_2$ = 0.045 g/g). ϕ_c = 0.3 vol. %. The lamp is switched off at time = 0 s. For 1 vol.%: σ_0 = 1.3×10^{-6} S cm^{-1}, 2 vol.%: σ_0 = 1.1×10^{-5} S cm^{-1}, 3.8 vol.%: σ_0 = 6.7×10^{-5} S cm^{-1}. (a) UV light. (b) Visible light.

(Sb 13%; MPS/Sb:SnO$_2$ ratio 0.045 g/g) as used for the photocatalytic experiments are discussed (Figure 9).

It has been shown earlier that the Sb:SnO$_2$ particles almost touch each other in the conductive network even when the surface of the particles is grafted with a monolayer of MPS [1]. By irradiation of the materials electron-hole splitting in the particle occurs, and probably the activated electron is transferred to a neighboring Sb:SnO$_2$ particle of the particle network. Apparently the distance between the particles is small enough to transfer the charge. The increase in the intensity of the plasmon reflection band during UV irradiation confirm this suggestion that at least part of the activated electrons are in the conduction band of the nanoparticles (Figure 2).

Figure 9(a) shows that the increase in σ under UV irradiation can be large and depends strongly on the concentration of the Sb:SnO$_2$ particles. Furthermore, it is likely to depend also on the amount of radiation absorbed and the morphology of the Sb:SnO$_2$ particle network. In absolute terms the maximum value of σ is about 1.2×10^{-3} S/cm (3.8 vol.%) which is close to the volume conductivity of the compressed Sb:SnO$_2$ powder used in these films, but is still a factor of ten lower than the intrinsic conductivity of these particles [31].

By using visible light also the occurrence of photo-conduction was observed (Figure 9(b)). This suggests that Sb:SnO$_2$ particles still may act as photocatalysts when the energy of the absorbed light quanta is not enough to excite an electron directly from the valence band to the conduction band. It was recently demonstrated that after N-doping of Sb:SnO$_2$ (Sb = 0%) the photodegradation of methylene blue under visible light illumination became possible [51]. The photocatalytic properties of the Sb:SnO$_2$ particles

(Sb ≥ 0%) for (meth)acrylate polymerization using incident light wavelengths above 340 nm are presently being studied.

The decays of σ after switching of the UV light shown in Figure 9 can be fitted well by a bifuntional exponential decay curve (Table 2). That the decrease in the concentration of the electrons activated by the absorption of light is relatively slow especially at a later stage of the reaction was also suggested by the slow decrease in intensity of the plasmon band observed with IR when the incident radiation was switched off (Figure 2).

In previous articles we reported the σ values of several cured MPS-Sb:SnO$_2$ (Sb > 0%)/acrylate layers. The samples were kept in the dark, and the measurements were performed under exclusion of incident UV/visible light to minimize the degradation of the polycarbonate supporting layer [1, 4, 52]. That incident light could enhance the σ of these materials was observed later on the first time.

4. Conclusions

4.1. Photocatalysis. Under a nitrogen atmosphere Sb:SnO$_2$ nanoparticles (0 ≤ Sb ≤ 13%) photocatalyze the polymerization of (meth)acrylate C=C bonds when incident radiation of 315 nm is used. The Sb:SnO$_2$ particles are welldispersed in the PEGDA 575 acrylate monomer when the particles are grafted in advance on the surface with the methacrylate silane coupling agent MPS. The photocatalytic conversion of the C=C bonds is complete and, a hard, transparent (>98%) crosslinked Sb:SnO$_2$/acrylate film with a low haze (<1%) is obtained after irradiation when MPS grafted particles doped with Sb are used in the PEGDA starting formulation. Without MPS grafting and Sb doping

the cured materials are no longer transparent, and these materials are inhomogeneous. Evidence is presented that in all the cured films the Sb:SnO$_2$ particles are chemically connected to the crosslinked matrix.

To our knowledge photocatalytic (meth)acrylate C=C polymerization by Sb:SnO$_2$ particles is never reported before. Therefore the photocatalytic conversions of a broad range of MPS-Sb:SnO$_2$/PEGDA 575 starting formulations were studied using real-time FT-IR spectroscopy, incident UV radiation of 315 nm and variable concentrations of Sb:SnO$_2$ nanoparticles with different Sb doping and MPS grafting level. These experiments show that

(i) The observed photocatalytic conversion rates of the C=C bonds can be explained quantitatively when MPS-grafted Sb:SnO$_2$(Sb > 0%) nanoparticles and a specific incident UV radiation of 315 nm with a small wavelength distribution are used.

(ii) By absorption of light quanta of 315 ± 5 nm the electrons of the valence bond of these nanoparticles are transferred directly into the conduction band, and the activated electron reacts with a (meth)acrylate C=C bond to form the initiating radical for C=C bond polymerization. The increase in activated electrons in the conduction band during irradiation is confirmed by an observed shift in peak position and/or increase in peak intensity of the plasmon band.

(iii) The quantum yield for this initiating radical formation (Φ) is for particles with Sb doping levels ≥2% independent of the amount of Sb:SnO$_2$ nanoparticles present. It decreases with an increase in MPS grafting on the particle surface. MPS grafting also lowers the relative quantum yield K by lowering the ratio between the polymer propagation and termination reaction rate constants.

(iv) Sb doping also lowers Φ, probably by lowering the amount of efficient hole scavengers initially present in Sb:SnO$_2$(Sb ≈ 0%) and by trapping the activated electrons present in the conduction band.

(v) When Sb:SnO$_2$ (Sb = 0%) particles are used in the starting acrylate monomer formulations photocatalyzed C=C bond polymerizations as well as unwanted photocatalyzed side reactions occur. These last ones are probably photocatalytically activated by the oxygen vacancies present in these nanoparticles.

4.2. Photoconduction. When transparent (>98%) semiconductive MPS-grafted Sb:SnO$_2$/(meth)acrylate cured composites are irradiated with UV or visible light the conductivities of these materials are increased. The increase in conductivity under UV irradiation in these composites can be very high and may reach the level of compressed Sb:SnO$_2$ nanopowder at particle concentrations of 4 vol. %. The occurrence of the conductivity increase can be explained by the absorption of light quanta by the Sb:SnO$_2$ nanoparticles present in the particle network. To our knowledge the occurrence of photoconduction in polymer composites containing (MPS)-Sb:SnO$_2$ (nano)particles (Sb ≥ 0%) is never reported before.

Acknowledgment

References

[1] V. A. Soloukhin, J. C. M. Brokken-Zijp, and G. De With, "Conductive ATO-acrylate nanocomposite hybrid coatings: experimental results and modeling," *Journal of Polymer Science. Part B*, vol. 45, no. 16, pp. 2147–2160, 2007.

[2] A. Wakabayashi, Y. Sasakawa, T. Dobashi, and T. Yamamoto, "Self-assembly of tin oxide nanoparticles: localized percolating network formation in polymer matrix," *Langmuir*, vol. 22, no. 22, pp. 9260–9263, 2006.

[3] Y. Wang and C. Anderson, "Formation of thin transparent conductive composite films from aqueous colloidal dispersions," *Macromolecules*, vol. 32, no. 19, pp. 6172–6179, 1999.

[4] W. E. Kleinjan, J. C. M. Brokken-Zijp, R. van de Belt, Z. Chen, and G. de With, "Antimony-doped tin oxide nanoparticles for conductive polymer nanocomposites," *Journal of Materials Research*, vol. 23, no. 3, pp. 869–880, 2008.

[5] J. Sun, W. W. Gerberich, and L. F. Francis, "Electrical and optical properties of ceramic-polymer nanocomposite coatings," *Journal of Polymer Science. Part B*, vol. 41, no. 14, pp. 1744–1761, 2003.

[6] A. Wakabayashi, Y. Sasakawa, T. Dobashi, and T. Yamamoto, "Optically transparent conductive network formation induced by solvent evaporation from tin-oxide-nanoparticle suspensions," *Langmuir*, vol. 23, no. 15, pp. 7990–7994, 2007.

[7] C. Damm, "An acrylate polymerisation initiated by iron doped titanium dioxide," *Journal of Photochemistry and Photobiology A*, vol. 181, no. 2-3, pp. 297–305, 2006.

[8] R. Ojah and S. K. Dolui, "Photopolymerization of methyl methacrylate using dye-sensitized semiconductor based photocatalyst," *Journal of Photochemistry and Photobiology A*, vol. 172, no. 2, pp. 121–125, 2005.

[9] A. J. Hoffman, H. Yee, G. Mills, and M. R. Hoffmann, "Photoinitiated polymerization of methyl methacrylate using Q-sized ZnO colloids," *Journal of Physical Chemistry*, vol. 96, no. 13, pp. 5540–5546, 1992.

[10] U. Gesenhues, "Al-doped TiO pigments: influence of doping on the photocatalytic degradation of alkyd resins," *Journal of Photochemistry and Photobiology A*, vol. 139, no. 2-3, pp. 243–251, 2001.

[11] L. Cao, F. J. Spiess, A. Huang et al., "Heterogeneous photocatalytic oxidation of 1-butene on SnO and TiO films," *Journal of Physical Chemistry B*, vol. 103, no. 15, pp. 2912–2917, 1999.

[12] B. R. Müller, S. Majoni, D. Meissner, and R. Memming, "Photocatalytic oxidation of ethanol on micrometer-and nanometer-sized semiconductor particles," *Journal of Photochemistry and Photobiology A*, vol. 151, no. 1–3, pp. 253–265, 2002.

[13] A. Mills and S. K. Lee, "A web-based overview of semiconductor photochemistry-based current commercial applications," *Journal of Photochemistry and Photobiology A*, vol. 152, no. 1–3, pp. 233–247, 2002.

[14] W. S. Tung and W. A. Daoud, "a new approach toward nanosized ferrous ferric oxide and iron-doped titanium dioxide photocatalysts," *ACS Applied Materials & Interfaces*, vol. 1, pp. 2453–2461, 2009.

[15] E. Martínez-Ferrero, Y. Sakatani, C. Boissière et al., "Nanostructured titanium oxynitride porous thin films as efficient visible-active photocatalysts," *Advanced Functional Materials*, vol. 17, no. 16, pp. 3348–3354, 2007.

[16] S. S. Pan, Y. X. Zhang, X. M. Teng, G. H. Li, and L. Li, "Optical properties of nitrogen-doped Sn O$_2$ films: effect of the electronegativity on refractive index and band gap," *Journal of Applied Physics*, vol. 103, no. 9, Article ID 093103, pp. 1–4, 2008.

[17] M. Batzill and U. Diebold, "The surface and materials science of tin oxide," *Progress in Surface Science*, vol. 79, no. 2–4, pp. 47–154, 2005.

[18] S. Shanthi, C. Subramanian, and P. Ramasamy, "Investigations on the optical properties of undoped, fluorine doped and antimony doped tin oxide films," *Crystal Research and Technology*, vol. 34, no. 8, pp. 1037–1046, 1999.

[19] D. J. Binks, D. P. West, S. Norager, and P. O'Brien, "Field-independent grating formation rate in a photorefractive polymer composite sensitized by CdSe quantum dots," *Journal of Chemical Physics*, vol. 117, no. 15, pp. 7335–7341, 2002.

[20] L. Ding, D. Jiang, J. Huang et al., "Photorefractive performance of a novel multifunctional inorganic-organic hybridized nanocomposite sensitized by CdS nanoparticles," *Journal of Physical Chemistry C*, vol. 112, no. 27, pp. 10266–10272, 2008.

[21] W. Posthumus, P. C. M. M. Magusin, J. C. M. Brokken-Zijp, A. H. A. Tinnemans, and R. Van Der Linde, "Surface modification of oxidic nanoparticles using 3- methacryloxypropyltrimethoxysilane," *Journal of Colloid and Interface Science*, vol. 269, no. 1, pp. 109–116, 2004.

[22] W. C. Hamilton, *Statistics in Physical Science*, Ronald Press, New York, NY, USA, 1964.

[23] Z. Y. Huang, T. Barber, G. Mills, and M. B. Morris, "Heterogeneous photopolymerization of methyl methacrylate initiated by small ZnO particles," *Journal of Physical Chemistry*, vol. 98, no. 48, pp. 12746–12752, 1994.

[24] A. L. Stroyuk, V. M. Granchak, A. V. Korzhak, and S. Y. Kuchmii, "Photoinitiation of buthylmethacrylate polymerization by colloidal semiconductor nanoparticles," *Journal of Photochemistry and Photobiology A*, vol. 162, no. 2-3, pp. 339–351, 2004.

[25] I. G. Popović, L. Katsikas, and H. Weller, "The photopolymerisation of methacrylic acid by colloidal semiconductors," *Polymer Bulletin*, vol. 32, no. 5-6, pp. 597–603, 1994.

[26] C. Decker and A. D. Jenkins, "Kinetic approach of O2 inhibition in ultraviolet- and laser-induced polymerizations," *Macromolecules*, vol. 18, no. 6, pp. 1241–1244, 1985.

[27] C. Decker and K. Moussa, "A new method for monitoring ultra-fast photopolymerizations by real-time infra-red (RTIR) spectroscop," *Die Makromolekulare Chemie*, vol. 189, no. 10, pp. 2381–2394, 1988.

[28] W. Posthumus, Ph.D. Thesis, Eindhoven University of Technology, Eindhoven, The Netherlands, 2004.

[29] D. Lin-Vien, N. B. Colthup, W. G. Fately, and J. G. Grasselli, *The Handbook of Infrared and Raman Characteristic Frequencies of Organic Molecules*, Academic Press, San Diego, Calif, USA, 1991.

[30] J. Guo, C. She, and T. Lian, "Ultrafast electron transfer between molecule adsorbate and antimony doped tin oxide (ATO) nanoparticles," *Journal of Physical Chemistry B*, vol. 109, no. 15, pp. 7095–7102, 2005.

[31] L. J. Huijbregts, H. B. Brom, J. C. M. Brokken-Zijp, W. E. Kleinjan, and M. A. J. Michels, "Dielectric quantification of conductivity limitations due to nanofiller size in conductive powders and nanocomposites," *Physical Review B*, vol. 77, no. 7, Article ID 075322, 2008.

[32] C. McGinley, H. Borchert, M. Pflughoefft et al., "Dopant atom distribution and spatial confinement of conduction electrons in Sb-doped SnO nanoparticles," *Physical Review B*, vol. 64, no. 24, Article ID 245312, pp. 1–9, 2001.

[33] T. Nütz, U. Zum Felde, and M. Haase, "Wet-chemical synthesis of doped nanoparticles: blue-colored colloids of n-doped SnO2:Sb," *Journal of Chemical Physics*, vol. 110, no. 24, pp. 12142–12150, 1999.

[34] T. Nütz and M. Haase, "Wet-chemical synthesis of doped nanoparticles: optical properties of oxygen-deficient and antimony-doped colloidal SnO2," *Journal of Physical Chemistry B*, vol. 104, no. 35, pp. 8430–8437, 2000.

[35] U. Zum Felde, M. Haase, and H. Weller, "Electrochromism of highly doped nanocrystalline SnO:Sb," *Journal of Physical Chemistry B*, vol. 104, no. 40, pp. 9388–9395, 2000.

[36] A. J. Hoffman, G. Mills, H. Yee, and M. R. Hoffmann, "Q-sized CdS: synthesis, characterization, and efficiency of photoinitiation of polymerization of several vinylic monomers," *Journal of Physical Chemistry*, vol. 96, no. 13, pp. 5546–5552, 1992.

[37] R. Mehnert, A. Pincus, I. Janorsky, R. Stowe, and A. Berejka, *UV & EB Curing Technology and Equipment*, vol. 1, John Wiley & Sons, Chichester, UK, 1998.

[38] G. R. Tryson and A. R. Shultz, "Calorimetric study of acrylate photopolymerization," *Journal of Polymer Science. Part A*, vol. 17, no. 12, pp. 2059–2075, 1979.

[39] J. F. G. A. Jansen, E. E. J. E. Houben, P. H. G. Tummers, D. Wienke, and J. Hoffmann, "Real-time infrared determination of photoinitiated copolymerization reactivity ratios: application of the Hilbert transform and critical evaluation of data analysis techniques," *Macromolecules*, vol. 37, no. 6, pp. 2275–2286, 2004.

[40] J. Brandrup, *Polymer Handbook*, 4th edition, 1999.

[41] J. D. Miller and H. Ishida, "Quantitative analysis of covalent bonding between substituted silanes and inorganic surfaces," *The Journal of Chemical Physics*, vol. 86, no. 3, pp. 1593–1600, 1987.

[42] Ç. Kiliç and A. Zunger, "Origins of coexistence of conductivity and transparency in SnO," *Physical Review Letters*, vol. 88, no. 9, Article ID 095501, pp. 1–4, 2002.

[43] C. S. Rastomjee, R. G. Egdell, M. J. Lee, and T. J. Tate, "Observation of conduction electrons in Sb-implanted SnO by ultraviolet photoemission spectroscopy," *Surface Science*, vol. 259, no. 3, pp. L769–L773, 1991.

[44] F. Gu, S. F. Wang, M. K. Lü, G. J. Zhou, D. Xu, and D. R. Yuan, "Photoluminescence properties of SnO nanoparticles synthesized by sol-gel method," *Journal of Physical Chemistry B*, vol. 108, no. 24, pp. 8119–8123, 2004.

[45] C. G. Fonstadt and R. H. Redicker, "Electrical properties of high-quality stannic oxide crystals," *Journal of Applied Physics*, vol. 42, no. 7, p. 2911, 1971.

[46] C. S. Rastomjee, R. G. Egdell, M. J. Lee, and T. J. Tate, "Observation of conduction electrons in Sb-implanted SnO by ultraviolet photoemission spectroscopy," *Surface Science*, vol. 259, no. 3, pp. L769–L773, 1991.

[47] F. E. Osterloh, "Inorganic materials as catalysts for photochemical splitting of water," *Chemistry of Materials*, vol. 20, no. 1, pp. 35–54, 2008.

[48] H. G. Kim, D. W. Hwang, and J. S. Lee, "An undoped, single-phase oxide photocatalyst working under visible light," *Journal of the American Chemical Society*, vol. 126, no. 29, pp. 8912–8913, 2004.

[49] R. Asahi, T. Morikawa, T. Ohwaki, K. Aoki, and Y. Taga, "Visible-light photocatalysis in nitrogen-doped titanium oxides," *Science*, vol. 293, no. 5528, pp. 269–271, 2001.

[50] K. L. Chopra, S. Major, and D. K. Pandya, "Transparent conductors—a status review," *Thin Solid Films*, vol. 102, no. 1, pp. 1–46, 1983.

[51] S. S. Pan, Y. D. Shen, X. M. Teng et al., "Substitutional nitrogen-doped tin oxide single crystalline submicrorod arrays: vertical growth, band gap tuning and visible light-driven photocatalysis," *Materials Research Bulletin*, vol. 44, no. 11, pp. 2092–2098, 2009.

[52] V. A. Soloukhin, J. C. M. Brokken-Zijp, O. L. J. Van Asselen, and G. De With, "Physical aging of polycarbonate: elastic modulus, hardness, creep, endothermic peak, molecular weight distribution, and infrared data," *Macromolecules*, vol. 36, no. 20, pp. 7585–7597, 2003.